PHYSICAL REVIEW A VOLUME 57, NUMBER 2 FEBRUARY 1998

Resonant dissociative photoionization of H_2 and D_2

I. Sánchez and F. Martín
Departamento de Química C-9, Universidad Autónoma de Madrid, 28049-Madrid, Spain

(Received 15 July 1997)

We present a theoretical study of dissociative photoionization of H_2 and D_2, with emphasis on resonant effects through intermediate doubly excited states. The theory coherently includes competition between the different dissociation and ionization channels, and makes use of *B*-spline functions to represent both the electronic and nuclear motions. We show that strong interference effects between resonant and nonresonant amplitudes are responsible for unidentified peaks observed in recent experimenal works, and that, for photon energies smaller than 28 eV, the various peaks can be explained in terms of a single $^1\Sigma_u^+$ doubly excited state. [S1050-2947(98)01102-0]

PACS number(s): 33.80.Eh, 33.80.Gj

I. INTRODUCTION

Dissociative photoionization of H_2 is the process in which a photon breaks the molecule into three fragments: $H + H^+ + e^-$. It plays a fundamental role in interstellar clouds, planetary atmospheres, and plasma physics. Historically, the first investigations of dissociative ionization were performed in the early 1970s by analyzing the kinetic-energy distribution (KED) of the resulting protons [1–8] and its angular dependence [9]. Experimental evidence of resonance effects was obtained by Strathdee and Browning [10], who observed a pronounced peak in the KED that they attributed to the lowest $^1\Sigma_u^+$ doubly excited state of H_2. This interpretation was later confirmed by theoretical calculations [11–13] that were able to reproduce both the position and the qualitative shape of the resonance peak. After a decade of slower progress (see Refs. [14,15] and references therein), improved experimental approaches have led to the discovery of new interesting features. For instance, very recently, Ito, Hall, and Ukai [16] reported the existence of several peaks in the KED of protons and deuterons produced via dissociative photoionization of molecular hydrogen and deuterium. These peaks were neither observed in previous works nor predicted theoretically, and, surprisingly, their positions do not seem to correspond to any known resonant state of H_2 or D_2. In a different experimental approach, He *et al.* [17] observed some structure in the zero ion kinetic-energy spectrum of H_2 in the region of low photon energies. The use of simple energy conservation arguments leads to the conclusion that this low-energy structure might correspond to a $^1\Sigma_g^+$ doubly excited state. However, this is very puzzling because the dipolar model, which should be valid for the radiation intensities reported in that work, does not allow excitation of a $^1\Sigma_g^+$ resonance. Finally, Latimer and co-workers [18,19] determined, from their measured KED spectra, autoionization widths for the lowest $^1\Sigma_u^+$ and $^1\Pi_u$ doubly excited states of H_2, in clear disagreement with the most recent theoretical calculations [20–23].

In a previous work [24], we showed that all these recent experimental observations can be explained as resulting from the strong interference between resonant and nonresonant dissociation processes. Here we explain the theoretical basis that supports the previous interpretation, and present a systematic study of resonant dissociative photoionization for H_2 and D_2. In particular, we present KED spectra in the photon energy range 25–28 eV, and total dissociative photoionization cross sections from the dissociation threshold ($\simeq 19$ eV) up to $\simeq 30$ eV. We will compare our results with the experimental ones of Refs. [16,17], and show that the interference effects described in Ref. [24] exist for a wide range of photon energies and for both H_2 and D_2.

Our theoretical method closely follows the pioneering ideas of Bardsley [25] and Hazi, Rescigno, and Kurilla [26]. These authors provided an appropriate theoretical framework to obtain a rigorous description of the electronic and nuclear motions, and the interference between them. In the present work we generalize this theoretical framework to study dissociative photoionization of H_2 and D_2. For this purpose we make use of *B*-spline functions [27] to represent both the electronic and nuclear wave functions. In a previous work [23], we showed that *B*-spline functions are able to provide accurate energy positions and autoionization widths for a large number of doubly excited states of H_2. We will show here that the use of *B* splines leads to a similar accurate description of the nuclear motion. The advantage of using *B* splines is that one avoids solving the complicated systems of integrodifferential equations that arise from the theory. This is essential to account for interference effects not included in previous theoretical works, and to explain the experimental findings.

The paper is organized as follows. In Sec. II we describe in detail the theoretical method and its relation with the usual approximations reported in the literature. Our implementation of the theory with *B*-spline functions is described in Sec. III. All the technical aspects of the calculations, such as convergence tests, accuracy of the results, etc., are given in Sec. IV. The results are presented and discussed in Sec. V. Finally, we end the paper with some conclusions in Sec. VI. Atomic units are used throughout unless otherwise stated.

II. THEORY

A. Photoionization cross section

In the following, we will assume that there is no interaction between vibrational and rotational motions, so that the

1050-2947/98/57(2)/1006(12)/$15.00

rotational wave functions can be factored out. Also, we will use the dipole approximation to describe the photon-molecule interaction. For the sake of comparison with experimental results, we will average the observable quantities upon all possible orientations. Under these conditions, the photoionization cross section for ionization from a single initial state $\Psi_{g\nu}$ is given by [28]

$$\sigma_{\alpha v}(E)=\frac{4\pi^2\omega}{3c}\sum_l \sum_m \sum_p \times\left|\int dR\langle\Psi_{g\nu}(\mathbf{r},R)|\mathbf{e}_p\cdot\mathbf{D}|\Psi^+_{\alpha v l m E}(\mathbf{r},R)\rangle\right|^2, \tag{1}$$

where g and ν indicate the initial electronic and vibrational state, respectively, ω is the photon energy, $\mathbf{e}_p$ is the photon polarization vector, $\mathbf{D}$ is either $\mathbf{r}_1+\mathbf{r}_2$ (length gauge) or $(\nabla_1+\nabla_2)/\omega$ (velocity gauge), and $\Psi^+_{\alpha v l m E}$ is the final state. In the latter state, the superscript $+$ indicates the usual outgoing boundary conditions in electron-molecule scattering; l is the angular momentum of the ejected electron and m its z component, $E=W_{g\nu}+\omega$, with $W_{g\nu}$ the total energy of the molecule in the initial state; and α and v denote, respectively, the electronic and vibrational states of the residual molecular ion. The index α includes all electronic quantum numbers of the residual ion and v stands for either bound or continuum vibrational states of the ion. The vector $\mathbf{r}$ labels all electronic coordinates, and R is the internuclear distance. In Eq. (1), and throughout the paper, integration over R is written explicitly, and integration over $\mathbf{r}$ is indicated with the usual bra-ket notation. As a consequence of the rotational average, Eq. (1) includes a sum over all possible polarization directions. Hence the photoionization cross section is the same for linearly and circularly polarized photons.

B. Initial and final states

Neglecting relativistic effects, the Hamiltonian of the H_2 molecule in the body-fixed frame can be decomposed according to

$$\mathcal{H}(\mathbf{r},R)=\mathcal{H}_{\mathrm{el}}(\mathbf{r},R)+T(R), \tag{2}$$

where $\mathcal{H}_{\mathrm{el}}$ is the usual electronic Hamiltonian which depends parametrically on R and contains all the potential-energy terms (including the nucleus-nucleus repulsion), and T is the relative kinetic energy of the nuclei,

$$T(R)=-\frac{1}{2\mu}\frac{d^2}{dR^2}+\frac{J(J+1)}{2\mu R^2}, \tag{3}$$

with μ denoting the reduced mass and J the total orbital angular momentum (electronic plus nuclear).

We assume that the initial state is well described in the framework of the Born-Oppenheimer (BO) approximation, i.e.,

$$\Psi_{g\nu}(\mathbf{r},R)=\psi_g(\mathbf{r},R)\chi_\nu(R), \tag{4}$$

where the electronic wave function satisfies

$$[\mathcal{H}_{\mathrm{el}}-E_g(R)]\psi_g(\mathbf{r},R)=0 \tag{5}$$

and the corresponding nuclear wave function

$$[T(R)+E_g(R)-W_{g\nu}]\chi_\nu(R)=0. \tag{6}$$

$E_g(R)$ is the BO potential-energy curve of the initial electronic state of the molecule. In the present work, the initial state will be the lowest $^1\Sigma_g^+$ electronic state of H_2 in the lowest vibrational state $\nu=0$. Therefore, application of the dipole selection rules to Eq. (1) implies that only electronic states of $^1\Sigma_u^+$ and $^1\Pi_u$ symmetries will be populated. Since we will only consider photoionization that leaves the $H_2{}^+$ ion in the $1s\sigma_g$ state, different values of m will not be coupled, so that we will drop the index m from now on. Also, due to our neglect of rotation-vibration interaction and to the rotational average, we will consider $J=0$ in the initial state.

In general, the final state $\Psi^+_{\alpha v l E}$ cannot be written in such a simple way as the initial state in Eq. (4). Indeed when the photon energy is large enough to populate doubly excited states of the molecule, the final-state wave function receives contributions from the nonresonant background as well as from the resonant doubly-excited states. This implies that a realistic description of the nuclear wave function must take into account the interference effects between the direct ionization and autoionization processes. Thus we assume that there is a set of orthogonal resonant states $\phi_r(\mathbf{r},R)$ embedded in the electronic continuum of H_2, and define two orthogonal projection operators

$$Q=\sum_{r'}|\phi_{r'}(\mathbf{r},R)\rangle\langle\phi_{r'}(\mathbf{r},R)| \tag{7}$$

and

$$P=1-Q. \tag{8}$$

The resonance energies are given by

$$E_r(R)\delta_{rr'}=\langle\phi_r|\mathcal{H}_{\mathrm{el}}|\phi_{r'}\rangle. \tag{9}$$

Then the complete final-state wave function can be written

$$\Psi^+_{\alpha v l E}=P\Psi^+_{\alpha v l E}+Q\Psi^+_{\alpha v l E}. \tag{10}$$

Using the definition of Q given in Eq. (7), we can write

$$Q\Psi^+_{\alpha v l E}=\sum_{r'}\phi_{r'}(\mathbf{r},R)\xi^{r'}_{\alpha v l E}(R), \tag{11}$$

where the functions $\xi^r_{\alpha v l E}(R)$ describe the relative motion of the nuclei when the system is in the ϕ_r resonant state. Substituting Eq. (10) in the Schrödinger equation

$$[\mathcal{H}(\mathbf{r},R)-E]\Psi^+_{\alpha v l E}(\mathbf{r},R)=0, \tag{12}$$

and projecting into P and Q subspaces, one obtains the system of coupled equations

$$(E-P\mathcal{H}P)P\Psi^+_{\alpha v l E}=P\mathcal{H}Q\Psi^+_{\alpha v l E}, \tag{13}$$

$$(E-Q\mathcal{H}Q)Q\Psi^+_{\alpha v l E}=Q\mathcal{H}P\Psi^+_{\alpha v l E}. \tag{14}$$

A formal solution of Eq. (13) can be written using the Lippman-Schwinger equation

$$P\Psi^{+}_{\alpha vlE}=P\Psi^{0+}_{\alpha vlE}+G^{+}_{P}(E)P\mathcal{H}Q\Psi^{+}_{\alpha vlE}\,, \tag{15}$$

where G^{+}_{P} is the Green's operator

$$G^{+}_{P}(E)=\lim_{\eta\to 0}\frac{1}{E-P\mathcal{H}P+i\eta}, \tag{16}$$

and $P\Psi^{0+}_{\alpha vlE}$ is the nonresonant scattering wave function that satisfies the equation

$$(P\mathcal{H}P-E)P\Psi^{0+}_{\alpha vlE}=0. \tag{17}$$

Substituting Eq. (15) into Eq. (14) one obtains an equation for the resonant wave function $Q\Psi^{+}_{\alpha vlE}$

$$(E-Q\mathcal{H}Q)Q\Psi^{+}_{\alpha vlE}=Q\mathcal{H}P[P\Psi^{0+}_{\alpha vlE}+G^{+}_{P}(E)P\mathcal{H}Q\Psi^{+}_{\alpha vlE}]. \tag{18}$$

Now we assume that the Born-Oppenheimer approximation is valid for both the resonance states $\phi_r(\mathbf{r},R)$ and the nonresonant continuum states $P\Psi^{+}_{\alpha vlE}$. This means that the BO approximation is valid within the P and Q subspaces,

$$[T(R),Q]=[T(R),P]=0, \tag{19}$$

and that the resonance-background coupling is due to the electronic interaction only, i.e.,

$$QT(R)P=PT(R)Q=0. \tag{20}$$

From Eq. (18), using Eqs. (11), (19), and (20), and projecting with $\phi_r(\mathbf{r},R)$ in the space of electronic coordinates, one obtains

$$\begin{aligned}[E-E_r(R)-T(R)]\xi^{r}_{\alpha vlE}(R)&=\langle\phi_r|Q\mathcal{H}_{\mathrm{el}}P|P\Psi^{0+}_{\alpha vlE}\rangle\\&\quad+\sum_{r'}\langle\phi_r|Q\mathcal{H}_{\mathrm{el}}PG^{+}_{P}(E)P\mathcal{H}_{\mathrm{el}}Q|\phi_{r'}\rangle\xi^{r'}_{\alpha vlE}(R).\end{aligned} \tag{21}$$

Now it is convenient to introduce the spectral resolution of $G^{+}_{P}(E)$,

$$G^{+}_{P}(E)=\lim_{\eta\to 0}\sum_{\alpha' l'}\sum\!\!\!\!\!\!\!\int_{v'}\sum\!\!\!\!\!\!\!\int dE'\times\frac{|P\Psi^{0+}_{\alpha' v' l' E'}(\mathbf{r},R)\rangle}{E-E'+i\eta}\int dR'\langle P\Psi^{0+}_{\alpha' v' l' E'}(\mathbf{r},R')|, \tag{22}$$

where $\sum\!\!\!\!\!\!\!\int dE'$ represents a sum over bound states and an integral over continuum states of the molecule, and $\sum\!\!\!\!\!\!\!\int_{v'}$ represents a sum over all bound *vibrational* states and an integral over all *dissociative* states (i.e., the vibrational continuum). Note that both integrals are not independent, and that E' is an upper bound for the integral in v'. Using the spectral resolution of $G^{+}_{P}(E)$, Eq. (21) can be written

$$\begin{aligned}[E-E_r(R)-T(R)]\xi^{r}_{\alpha vlE}(R)&=V^{r}_{\alpha vlE}(R)+\lim_{\eta\to 0}\sum_{r'}\sum_{\alpha' l'}\sum\!\!\!\!\!\!\!\int_{v'}\sum\!\!\!\!\!\!\!\int dE'\\&\quad\times\frac{V^{r}_{\alpha' v' l' E'}(R)}{E-E'+i\eta}\int dR'\,V^{r'\,*}_{\alpha' v' l' E'}(R')\xi^{r'}_{\alpha vlE}(R'),\end{aligned} \tag{23}$$

where

$$V^{r}_{\alpha vlE}(R)=\langle\phi_r|Q\mathcal{H}_{\mathrm{el}}P|P\Psi^{0+}_{\alpha vlE}\rangle\;. \tag{24}$$

For the case of an isolated resonance, Eq. (23) reduces to that proposed by Bardsley [25] and Hazi, Rescigno, and Kurilla [26]. It represents the nuclear motion when the electrons are in a quasistationary state ϕ_r. The matrix element in Eq. (24) represents the coupling between the resonance state and the nonresonant wave function of energy E and vibrational state v. Hence the two terms on the right-hand side of Eq. (23) are the result of the autoionizing character of the ϕ_r state. In particular, the last term represents the decay of the resonant state to the adjacent electronic continuum. This term is nonlocal due to the presence of the $\xi^{r}_{\alpha vlE}$ functions, and it can be split into the usual δ-function term and principal value term using

$$\lim_{\eta\to 0}\frac{1}{E-E'+i\eta}=-i\pi\delta(E-E')+\mathrm{P}\frac{1}{E-E'}. \tag{25}$$

Equation (23) is exact in the framework of the Born-Oppenheimer approximation. Within this approximation $P\Psi^{0+}_{\alpha vlE}$ can also be written as a product of electronic and nuclear wave functions,

$$P\Psi^{0+}_{\alpha vlE}(\mathbf{r},R)=\psi^{0+}_{\alpha l\epsilon}(\mathbf{r},R)\chi_v(R), \tag{26}$$

where $\psi^{0+}_{\alpha l\epsilon}(\mathbf{r},R)$ is the nonresonant electron-scattering wave function for a fixed position of the nuclei. It satisfies the equation

$$[P\mathcal{H}_{\mathrm{el}}(\mathbf{r},R)P-\mathcal{E}(R)]\psi^{0+}_{\alpha l\epsilon}(\mathbf{r},R)=0, \tag{27}$$

with $\mathcal{E}(R)=E_0(R)+\epsilon$, where $E_0(R)$ is the BO potential-energy curve of the residual ion and ϵ is the kinetic energy of the outgoing electron. The corresponding nuclear wave function χ_v is the solution of the equation

$$[T(R)+E_0(R)-W_v]\chi_v(R)=0, \tag{28}$$

where W_v is the energy of the residual ion and

$$E=\epsilon+W_v\,. \tag{29}$$

Equation (26) is often called, in the context of electron-molecule scattering theory, the *adiabatic nuclei approximation* [29]. It results from the validity of the BO approximation for both the molecule and the residual molecular ion, and from the boundary conditions that impose that the latter ion remains in a final vibrational state v. From the previous equation, the matrix element of Eq. (24) is given by

$$V^{r}_{\alpha vlE}(R)=\langle\phi_r|Q\mathcal{H}_{\mathrm{el}}P|\psi^{0+}_{\alpha l\epsilon}\rangle\chi_v(R). \tag{30}$$

Using Eqs. (15), (22), and (26), the total wave function defined in Eq. (10) can be written

$$\begin{aligned}\Psi^{+}_{\alpha vlE}(\mathbf{r},R)=&\sum_{r'}\phi_{r'}(\mathbf{r},R)\xi^{r'}_{\alpha vlE}(R)+\psi^{0+}_{\alpha l\epsilon}(\mathbf{r},R)\chi_v(R)\\ &+\lim_{\eta\to 0}\sum_{r'}\sum_{\alpha' l'}\sum\!\!\!\!\!\!\!\int_{v'}\sum\!\!\!\!\!\!\!\int dE'\\ &\times\frac{1}{E-E'+i\eta}\int dR' V^{r'\,*}_{\alpha' v' l' E'}(R')\\ &\times\xi^{r'}_{\alpha vlE}(R')\psi^{0+}_{\alpha' l'\epsilon'}(\mathbf{r},R)\chi_{v'}(R),\end{aligned} \tag{31}$$

with $E=\epsilon+W_v$ in the second term and $E'=\epsilon'+W_{v'}$ in the third one.

C. Relation with previous works

As mentioned above, Eq. (23) generalizes the method of Bardsley [25] and Hazi, Rescigno and Kurilla [29] to the case of several resonances. Another difference comes from the fact that we have employed the usual partial-wave expansion in electron-molecule scattering, while in the previous works the authors made use of a single molecular continuum which includes, in principle, the contribution from different partial waves. Although the latter procedure may seem more simple than the partial-wave expansion, practical calculations are in fact cumbersome since discretized representations of the ''true'' molecular continuum are not easy to obtain. Furthermore, the fact that Eq. (23) is nonlocal has prevented one from obtaining a rigorous solution of the nuclear motion within the BO approximation. Thus most previous works are based on the local approximation, which can be obtained from Eq. (23) in the following way. First we assume that there is a single isolated resonance ϕ_r, so that the sum over the index r' reduces to a single term. This is a reasonable approximation provided that, for all R, the energy separation between doubly excited states is much larger than the corresponding autoionization widths. Next we assume that the electron energy ϵ is much larger than the vibrational spacing $\Delta W=W_{v+1}-W_v$. This implies that the $\langle\phi_r|Q\mathcal{H}_{\mathrm{el}}P|\psi^{0+}_{\alpha l\epsilon}\rangle$ matrix elements do not vary significantly with v' (or, equivalently, with ϵ), so that they can be extracted from the integral $\sum\!\!\!\!\!\!\int_{v'}$ in the last term of Eq. (23). Finally, if contribution from the closed vibrational channels is negligible, we can write

$$\sum\!\!\!\!\!\!\!\int_{v'}|\chi_{v'}\rangle\langle\chi_{v'}|\simeq\sum\!\!\!\!\!\!\!\int_{v'}^{\infty}|\chi_{v'}\rangle\langle\chi_{v'}|=\delta(R-R'), \tag{32}$$

and Eq. (23) becomes

$$\begin{aligned}&\left[E-E_r(R)-\delta E_r(R)+\frac{i}{2}\Gamma_r(R)-T(R)\right]\xi^{r}_{\alpha vlE}(R)\\ &\quad=V^{r}_{\alpha vlE}(R),\end{aligned} \tag{33}$$

where $\delta E_r(R)$ and $\Gamma_r(R)$ are, respectively, the energy shift

$$\delta E_r(R)=\sum_{\alpha' l'}\mathcal{P}\sum\!\!\!\!\!\!\!\int d\epsilon'\frac{|\langle\phi_r|Q\mathcal{H}_{\mathrm{el}}P|\psi^{0+}_{\alpha' l'\epsilon'}\rangle|^2}{\epsilon_r-\epsilon'} \tag{34}$$

and the autoionization width

$$\Gamma_r(R)=2\pi\sum_{\alpha' l'}|\langle\phi_r|Q\mathcal{H}_{\mathrm{el}}P|\psi^{0+}_{\alpha' l'\epsilon_r}\rangle|^2 \tag{35}$$

of the resonance r. Note that in Eqs. (34) and (35), ϵ_r is the local electron energy $\epsilon_r=E_r(R)-E_0(R)$. Equation (33) is a local second-order differential equation much easier to solve than the original nonlocal equation (23). It was derived by Bardsley [25] and Hazi, Rescigno, and Kurilla [29], and used by Kirby *et al.* [12] to study dissociative photoionization of H_2 near the lowest ${}^1\Sigma_u^+$ doubly excited state. Several authors [26] made the additional assumption that the inhomogeneous term can be approximately written $V^{r}_{\alpha vlE}(R)\simeq[\Gamma_r(R)/2\pi]^{1/2}\chi_v$, which is a reasonable approximation when a single partial wave dominates the process.

Using the same approximations that led to Eq. (33), the total wave function given in Eq. (31) can be written

$$\begin{aligned}\Psi^{+}_{\alpha vlE}(\mathbf{r},R)=&\,\phi_r(\mathbf{r},R)\xi^{r}_{\alpha vlE}(R)+\psi^{0+}_{\alpha l\epsilon}(\mathbf{r},R)\chi_v(R)\\ &+\lim_{\eta\to 0}\sum_{\alpha' l'}\sum\!\!\!\!\!\!\!\int d\epsilon'\frac{1}{\epsilon_r-\epsilon'+i\eta}\\ &\times\langle\phi_r|Q\mathcal{H}_{\mathrm{el}}P|\psi^{0+}_{\alpha' l'\epsilon'}\rangle^{*}\psi^{0+}_{\alpha' l'\epsilon'}(\mathbf{r},R)\xi^{r}_{\alpha vlE}(R).\end{aligned} \tag{36}$$

Contributions arising from the last term in Eq. (36) have not been included in previous works. In this respect, we will show below that the approximation

$$\Psi^{+}_{\alpha vlE}(\mathbf{r},R)=\phi_r(\mathbf{r},R)\xi^{r}_{\alpha vlE}(R)+\psi^{0+}_{\alpha l\epsilon}(\mathbf{r},R)\chi_v(R) \tag{37}$$

is not a good one, and that inclusion of all the terms in Eq. (36) is essential for the validity of the local approximation.

III. COMPUTATIONAL METHODS

A. Electronic wave functions

We define an interval $[0,r_{\max}]$ and a basis of one-electron functions,

$$f_{ilm}(\mathbf{r})=r^{-1}B_i^k(r)Y^{lm}(\hat{r}), \tag{38}$$

where $Y^{lm}(\hat{r})$ is a spherical harmonic and B_i^k is the ith B spline of order k [27]. The B_i^k functions are piecewise polynomials of degree $k-1$ and are distributed along a knot sequence defined in the $[0,r_{\max}]$ interval. Additional knot points are defined in the borders of the interval, so that $B_i^k(0)=B_i^k(r_{\max})=0$ for all i, which is equivalent to enclosing the system in a box of size $r_{\max}$. The $H_2{}^+$ orbitals, φ_{nm}, are obtained by diagonalizing the $H_2{}^+$ Hamiltonian in the above basis, hence they are written

$$\varphi_{nm}=\frac{1}{r}\sum_{l=0}^{l_{\max}}\left[\sum_{i=1}^{N}a_i^{nl}B_i^k(r)\right]Y^{lm}(\hat{r}). \tag{39}$$

In this work we have used $k=8$, $r_{\max}=60$ a.u., $N=140$, and a linear knot sequence. We have included angular momenta up to $l_{\max}=8$. Since we have 140 B-spline functions per angular momentum, σ_g orbitals are expansions of 700 terms ($l=0$, 2, 4, 6, and 8), σ_u orbitals of 560 terms ($l=1$, 3, 5, and 7), π_g orbitals of 560 terms ($l=2$, 4, 6, and 8), and so on. Notice that as the spherical harmonics in Eq. (39) are placed on the nuclear center of mass, the number of l values required to achieve converged ${H_2}^+$ states is rather large. The present basis set has allowed us to perform calculations in the range $R=0-5$ a.u. (see Ref. [30]).

We have used the resonant wave functions ϕ_r obtained in our previous works for the ${}^1\Sigma_u^+$ and ${}^1\Pi_u$ symmetries [23,30]. They were obtained by diagonalizing the H_2 Hamiltonian in a basis of configurations built from the ${H_2}^+$ orbitals φ_{nm} mentioned above. For example, in the case of the ${}^1\Sigma_u^+$ symmetry, the expansion included 200 configurations ($\sigma_g\sigma_u$, $\pi_g\pi_u$, and $\delta_g\delta_u$), in which the lowest ${H_2}^+$ orbital, $1s\sigma_g$, was excluded in order to ensure orthogonality with the P subspace.

The continuum wave functions $\psi^{0+}_{\alpha l\epsilon}$ have been evaluated using the L^2 close-coupling approach [31]. For each channel αl, we have defined a set of orthogonal uncoupled continuum states (UCS's) in the static exchange approximation

$$\zeta^0_{\alpha l\epsilon}(\mathbf{r}_1,\mathbf{r}_2)=\Theta(\Phi_{\alpha l}(\mathbf{r}_1,\hat{r}_2)\varrho_{\alpha l\epsilon}(r_2)), \tag{40}$$

where Θ is the symmetrization operator (we only consider singlet states), $\varrho_{\alpha l\epsilon}$ is the radial wave function of the continuum electron, and $\Phi_{\alpha l}$ is the channel function, which is a state of ${H_2}^+$ combined with the angular function of the scattered electron to give the correct channel symmetry. In this work we have used the UCS's of Ref. [30], which were built using our calculated $1s\sigma_g$ orbital for ${H_2}^+$ and a radial continuum wave function expanded in a B-spline basis with well-defined angular momentum l. This procedure leads to a discrete spectrum $\{\epsilon_{\alpha l n}\}$ and to discretized UCS wave functions $\tilde{\zeta}^0_{\alpha l n}$ that have been renormalized using the appropriate density of states. We have evaluated all αl open channels with angular momentum up to $l=7$. As in Ref. [30], interchannel coupling between the UCS's has been introduced using a Lippman-Schwinger equation [31]. The corresponding Green's function has been evaluated as described by Martín [32]. All these wave functions have provided accurate energy positions and widths for the H_2 resonances (see Ref. [23] for a detailed comparison with previous works).

Finally, the ground state of the H_2 molecule has been evaluated using a one-electron orbital basis that contains $1s\sigma_g$ and $2s\sigma_g$ molecular orbitals, and Slater-type orbitals $r^{n-1}\exp(-\gamma_{il}r)$, which have been expanded over the same B-spline basis. The two-electron Hamiltonian has then been diagonalized in a basis of two-electron configurations, up to a number of 400.

B. Nuclear wave functions

The initial vibrational wave function is written as a linear combination of B-spline functions B_j^k of order k,

$$\chi_\nu(R)=R^{-1}\sum_j d_{\nu j}B_j^k(R). \tag{41}$$

The coefficients $d_{\nu j}$ are obtained by diagonalizing Eq. (6) in the B_j^k basis. The B splines are defined in an interval $[0,R_{\max}]$. The knot sequence is linear with additional knot points in the borders so that $B_i(0)=B_i(R_{\max})=0$ for all i. Here we have used 240 B splines with $k=8$ and $R_{\max}=12$ a.u.

We use the same procedure to obtain the χ_v vibrational functions associated with the nonresonant electronic continuum state [see Eq. (28)]. This leads to both bound vibrational states and discretized vibrational states $\tilde{\chi}_v$ with energies $\tilde{W}_v$ that satisfy

$$[T(R)+E_0(R)-\tilde{W}_v]\tilde{\chi}_v(R)=0, \tag{42}$$

with

$$\langle\tilde{\chi}_v|\tilde{\chi}_{v'}\rangle=\delta_{vv'}\,. \tag{43}$$

The continuum vibrational states normalized to a δ function on the energy scale are then given by

$$\chi_v(R)=\rho^{1/2}(\tilde{W}_v)\tilde{\chi}_v(R), \tag{44}$$

where ρ is the density of states which can be approximately written

$$\rho(\tilde{W}_v)=\frac{2}{\tilde{W}_{v+1}-\tilde{W}_{v-1}}. \tag{45}$$

The most difficult part is the evaluation of the $\xi^r_{\alpha lvE}$ wave functions from Eq. (23). These functions contain information about the interference between the resonant and nonresonant dissociation processes. At photon energies for which resonant effects in H_2 are observed, the $\xi^r_{\alpha lvE}$ functions oscillate strongly. Moreover, Eq. (23) is nonlocal, i.e., it couples the $\xi^r_{\alpha vlE}$ functions associated to different channels and different energies. For these reasons, a numerical solution of Eq. (23) is very difficult and much slower than an algebraic solution using an expansion in a finite state basis. We have defined such a basis as the eigenfunctions resulting from the diagonalization of the Schrödinger equation

$$[T(R)+E_r(R)-\mathcal{W}_k]\tilde{\Upsilon}_k(R)=0 \tag{46}$$

in the basis of B-spline functions indicated above. Then we use the $\{\tilde{\Upsilon}_k\}$ functions to expand $\xi^r_{\alpha vlE}$. Substituting

$$\xi^r_{\alpha vlE}(R)=\sum_i c^{r,i}_{\alpha vlE}\tilde{\Upsilon}_i(R) \tag{47}$$

into Eq. (23), projecting into the $\tilde{\Upsilon}_k$ functions, and using Eq. (46), one obtains the system of linear equations

$$\sum_i c^{r,i}_{\alpha vlE}[(E-\mathcal{W}_i)\delta_{ij}-\mathcal{D}^r_{ji}]=\mathcal{B}^{r,j}_{\alpha vlE}\,, \tag{48}$$

with

$$\mathcal{D}^{r}_{ji}=\lim_{\eta\to 0}\sum_{r'}\sum_{\alpha' l'}\sum\!\!\!\!\!\!\!\int_{v'}^{\infty}\sum\!\!\!\!\!\!\!\int dE' \times\frac{1}{E-E'+i\eta}\int dR'\tilde{\Upsilon}^{*}_{j}(R')V^{r}_{\alpha' v' l' E'}(R') \times\int dR'' V^{r'\,*}_{\alpha' v' l' E'}(R'')\tilde{\Upsilon}_{i}(R'') \tag{49}$$

and

$$\mathcal{B}^{r,j}_{\alpha v l E}=\int dR'\tilde{\Upsilon}^{*}_{j}(R')V^{r}_{\alpha v l E}(R'), \tag{50}$$

which provides the unknown coefficients $c^{r,i}_{\alpha v l E}$. In the previous equation, the integral over v' (the continuum part of the vibrational spectrum) was performed using the quadrature provided by the discrete energy eigenvalues $\tilde{W}_{v'}$ of Eq. (42). This is a standard procedure used in many different situations involving the vibrational continuum of a molecule [7,33]. It implies that the v' integral is replaced by a sum over discretized levels, and that the $V^{r}_{\alpha v l E}(R)$ matrix elements are replaced by $\tilde{V}^{r}_{\alpha v l E}(R)=\langle\phi_r|Q\mathcal{H}_{\rm el}P|\psi^{0+}_{\alpha l \epsilon}\rangle\tilde{\chi}_v(R)$ [see Eq. (24)]. The integral over E' is performed numerically in a grid $\{E'_k\}$ with a sufficiently small step size $\Delta E'_k$. In order to evaluate the contribution arising from the pole, the grid is chosen so that the pole condition $E=E'$ is satisfied exactly by one of the grid points. The values of ϵ' that are compatible with both the quadrature in v' and E' are obtained from the energy conservation condition $E'_k=\epsilon'_k+\tilde{W}_{v'}$ [see Eq. (29)]. In general, the discretization procedure that we used to evaluate the electronic continuum wave function yields a discrete energy spectrum that is different from the $\{\epsilon'_k\}$ one resulting from the previous condition. This problem is solved in practice by simply interpolating the calculated $V^{r}_{\alpha v l E}(R)$ matrix elements to the required energy. The same double-quadrature procedure has been used to evaluate the last term in Eq. (31). Convergence of the results can be checked by both decreasing $\Delta E'_k$ and increasing the density of continuum vibrational states. The latter can be achieved by enlarging the box where the B-spline basis is defined.

IV. CALCULATIONS

As mentioned above, the electronic wave functions used in the present work were taken from Refs. [23,30], in which convergence of various electronic properties was discussed in detail. Figure 1 shows the potential-energy curves that are relevant for the present study. Since resonance effects for photon energies smaller than 30 eV are expected to be dominated by the lowest doubly excited states, in all calculations presented here we have included only the lowest ${}^1\Sigma^+_u$ state and the lowest ${}^1\Pi_u$ one. These states also have the largest autoionization widths. They lie above the ionization threshold at short and intermediate internuclear distances. At $R=R_c$, their energies cross the ionization threshold, and the states lose their autoionizing character. (For instance, the lowest ${}^1\Sigma^+_u$ resonance, which is mainly described by a $2p\sigma_u 2s\sigma_g$ configuration, crosses the $1s\sigma_g$ ionization threshold at $R_c\simeq 4.1$ a.u.). As R increases, the resonance states cross the $1s\sigma_g nl\lambda$ Rydberg series and dissociate into H(1s)+H($n\geqslant 2$). However, these dissociation limits are not well described by our calculated ϕ_r states. Indeed, the partition of the problem into orthogonal P and Q subspaces implies that all configurations containing the $1s\sigma_g$ orbital of ${H_2}^+$ are excluded from the Q subspace. In the region of long internuclear distances this procedure leads to states with equal contributions from covalent H+H configurations and ionic $H^+ + H^-$ configurations. Hence the calculated states can never yield the correct dissociation limit H(1s)+H($n\geqslant 2$). In order to solve this difficulty at long internuclear distances, we used the diabatic potential-energy curves calculated by Borondo, Macías, and Riera [34] for $R>6.0$ a.u. These curves tend to the correct dissociation limit, and have been smoothly connected to our results for $R\leqslant 5.0$ a.u. The diabatic states of Ref. [34] were obtained by diagonalizing the matrix of nonadiabatic couplings in a basis containing the lowest adiabatic states of the same symmetry (e.g., three states in the case of the ${}^1\Sigma^+_u$ symmetry). Since autoionization below the threshold is not allowed, all electronic matrix elements involving the interaction between these diabatic states and the nonresonant states $\psi^{0+}_{\alpha l \epsilon}$ have been made zero beyond R_c. Also, in Eqs. (23) and (31) we replaced $\sum\!\!\!\!\!\!\int dE'$ by $\int dE'$, i.e., excluded summation over bound electronic states because contributions from the latter to the ionization process is expected to be negligible.

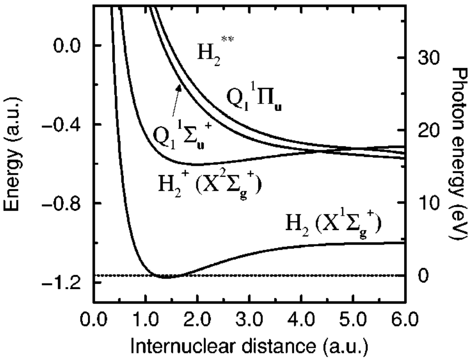

FIG. 1. Potential-energy curves of H_2 and ${H_2}^+$.

Now we focus on the accuracy of the calculated nuclear wave functions as well as on the resulting photoionization cross sections. First we analyze the accuracy of the method that consists in expanding the nuclear wave function $\xi^{r}_{\alpha v l E}(R)$ in an L^2 basis $\{\tilde{\Upsilon}_i(R)\}$ built from B-spline functions. For this purpose one has to compare with results obtained from numerical calculations. Since the latter are very difficult to perform using Eq. (23) directly, we have carried out such a test in the framework of the local approximation discussed in Sec. II C [see Eq. (33)]. In Fig. 2 we present the nuclear wave function $\xi^{r}_{\alpha v l E}(R)$ associated with the lowest ${}^1\Sigma^+_u$ doubly excited state, calculated by solving Eq. (33) both numerically and using an expansion over the $\tilde{\Upsilon}_i(R)$ basis. The plotted wave function corresponds to $E=-0.1723$ a.u. (i.e., $\omega=27$ eV) and $W_v=-0.3824$ a.u., and has been obtained for the dominant $l=1$ partial wave (see below). The numerical solution has been obtained using a standard Numerov method following a procedure described by Allison [35]. The $\tilde{\Upsilon}_i(R)$ basis has been represented using B-spline functions, as explained in Sec. II B. Then we solved

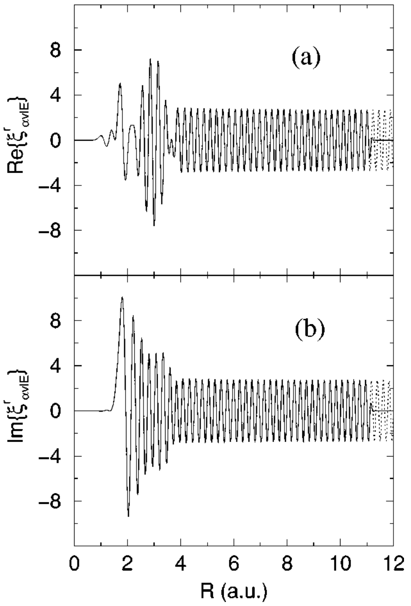

FIG. 2. Nuclear wave function $\xi^r_{\alpha vlE}$ of H_2 for $E=-0.1723$ a.u. (i.e., $\omega=27$ eV) and $W_v=-0.3824$ a.u. (i.e., 1.6-eV protons) obtained in the local approximation. Dotted line: numerical solution of Eq. (33); full line: algebraic solution in a B-spline basis using an absorbing potential (see text). (a) Real part. (b) Imaginary part.

Eq. (33) using the method described in Sec. III B. In order to avoid unphysical border effects due to the presence of the artificial potential wall placed at $R=R_{\max}$, we included a short-range absorbing potential in the close vicinity of $R=R_{\max}$. Introduction of this potential has no influence on the description of the inner part of the wave functions, but is essential in order to fulfill the asymptotic behavior given in Eq. (A1) (see the Appendix for a more detailed discussion). Complex absorbing potentials have been widely used in many other contexts, and applications are well documented in the literature [36]. Figure 2 shows that the wave functions calculated with B splines are indistinguishable from the numerical ones except, of course, in the vicinity of $R=R_{\max}$. The L^2 wave functions go to zero near $R_{\max}$, thus implying that the procedure is accurate provided that the interval $[0,R_{\max}]$ contains the relevant interactions. Hence a good check of the accuracy is invariance of the results when the box length is increased.

We also analyzed convergence of the results with respect to the number of angular momenta included in Eq. (1). In Fig. 3 we show the contribution of the different terms for the $^1\Sigma_u^+$ final symmetry and a photon energy $\omega=20$ eV. It can be observed that convergence is achieved very rapidly: the term corresponding to $l=1$ is nearly three orders of magnitude larger than that corresponding to $l=3$. This is so for all photon energies investigated in this work. Hence, in order to simplify the present calculations to a reasonable amount of computer time, we have only retained the leading term ($l=1$) to obtain all the results presented in Sec. V. Figure 3 shows that results obtained in this way will be affected by an error of 0.5% or less. It must be stressed here that this procedure is not equivalent to the usual static exchange approximation, which assumes that the outgoing electron is always in an $l=1$ continuum orbital [11]. Indeed, as mentioned above, our method allows for interchannel coupling between different partial waves, i.e., the incoming (outgoing) electron in the $l=1$ partial wave leads to outgoing (incoming) electrons in all partial waves included in the basis. Therefore, inelastic scattering from $l=1$ to $l'\neq 1$ is included in the present calculations. In the present work, l' goes from 0 up to $l_{\max}=8$.

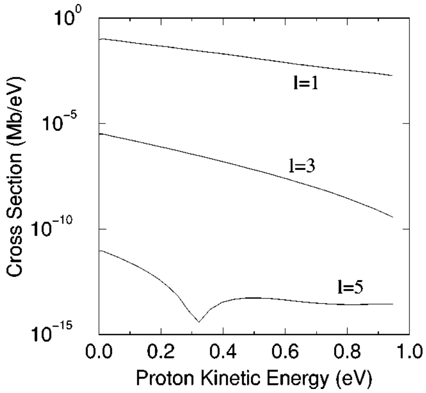

FIG. 3. Contribution of the different partial waves to the $^1\Sigma_u^+$ dissociative photoionization cross section of H_2 at $\omega=20$ eV.

We have also checked the accuracy of the quadrature procedure explained in Sec. III by increasing the value of $R_{\max}$. In all cases, the energy integrals have been performed using $\Delta E'=0.01$ a.u. In Fig. 4 we show the cross sections obtained for two different values of $R_{\max}$. The effect of enlarging the box from $R_{\max}=6$ a.u. to $R_{\max}=12$ a.u. is only to provide more points in the resulting cross section. We can see in the figure that the interpolated cross sections are practically indistinguishable for all values of the proton kinetic energy. This means that the cross sections for dissociative photoionization are practically converged for $R_{\max}=12$ a.u. Incidentally, cross sections for photoionization that leave the $H_2{}^+$ ion in a bound vibrational state are also converged for the lowest values of v. For high v, the value of $R_{\max}$ could be probably too small (the outer turning point is very far), but this would not be a serious constraint to evaluate total photoionization cross sections because the contribution from the region just below the dissociation threshold is very small [37].

Finally, some comments are appropriate concerning the

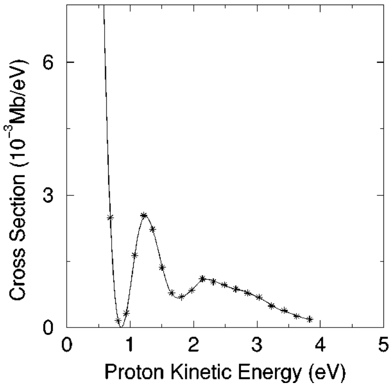

FIG. 4. Invariance of the $^1\Sigma_u^+$ dissociative photoionization cross sections with the size of the box $R_{\max}$ used to define the nuclear B-spline basis. Full line: $R_{\max}=12$ a.u.; stars: $R_{\max}=6$ a.u. The photon energy is 26 eV.

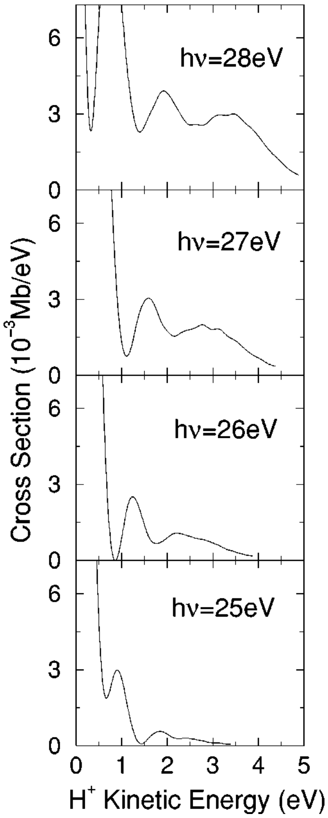

FIG. 5. KED spectra of H_2 for protons detected at 0° ($^1\Sigma_u^+$ contribution).

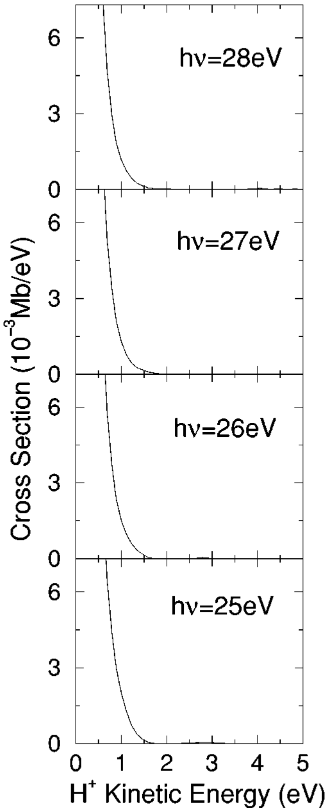

FIG. 6. KED spectra of H_2 for protons detected at 90° ($^1\Pi_u$ contribution).

invariance of the cross sections with respect to the gauge used in the calculations. In Ref. [30] we checked that, in the fixed nuclei approximation, the electronic wave functions led to converged results in the velocity gauge. Although we did not try to reach convergence in the length gauge, the cross sections obtained in the latter gauge differed by less than 10%. Therefore, for the sake of consistency, all the results presented in the following sections have been obtained using the velocity gauge. It must be recalled here that, since we are using the Born-Oppenheimer approximation, results obtained with the length and velocity gauges will never be identical. However, the differences are usually very small in the framework of this approximation, so that computation of cross sections using a single gauge is still meaningful (see Ref. [28] for a detailed discussion).

V. RESULTS AND DISCUSSION

A. Differential cross sections

In Figs. 5 and 6 we show the calculated KED of protons for the $^1\Sigma_u^+$ and $^1\Pi_u$ final symmetries of H_2 in the photon energy range $\omega = 25$–28 eV. Results for the D_2 molecule are shown in Figs. 7 and 8. As is well known [9], for protons and deuterons observed at 0° with respect to the polarization vector of the incident radiation, the only contribution to the cross section comes from the $^1\Sigma_u^+$ continuum, whereas for 90° only the $^1\Pi_u$ continuum is observed. For this reason, in Fig. 9 we compare the calculated $^1\Sigma_u^+$ cross section with the spectra measured by Ito, Hall, and Ukai [16] at 0°. We do not present any comparison at 90° because no resonant structure is observed either in our results or in the experiments.

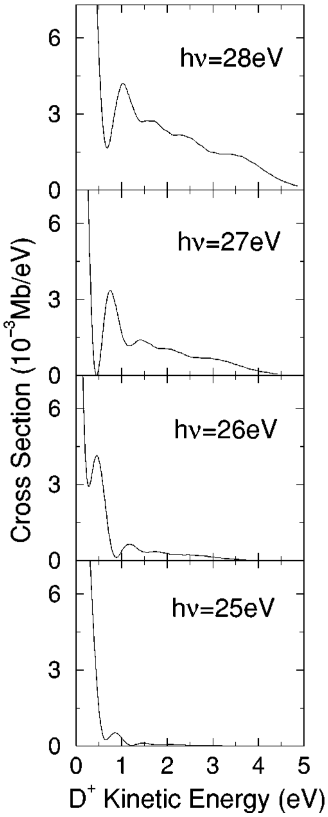

FIG. 7. KED spectra of D_2 for deuterons detected at 0° ($^1\Sigma_u^+$ contribution).

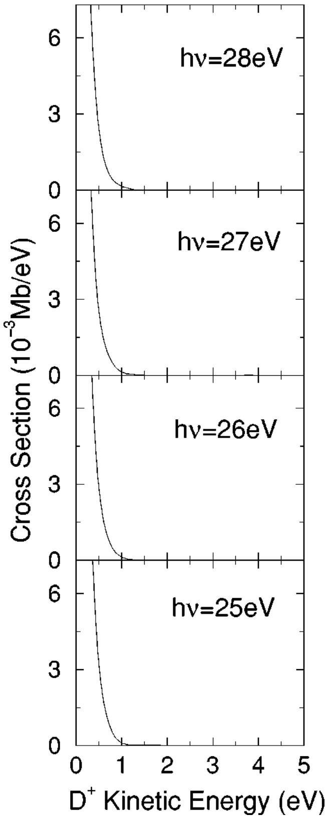

FIG. 8. KED spectra of D_2 for deuterons detected at 90° ($^1\Pi_u$ contribution).

The comparison is made at $\omega=27$ eV and, since the measurements are not given in an absolute scale, we have normalized the experimental spectra to the calculated values at 3 eV. Agreement between theory and experiment is good. We have not tried to obtain results at photon energies higher than 28 eV, because doubly excited states not included in our calculations begin to be populated. In fact, the agreement between our results and those of Ref. [16] at $\omega=28$ eV is worse than at 27 eV and below.

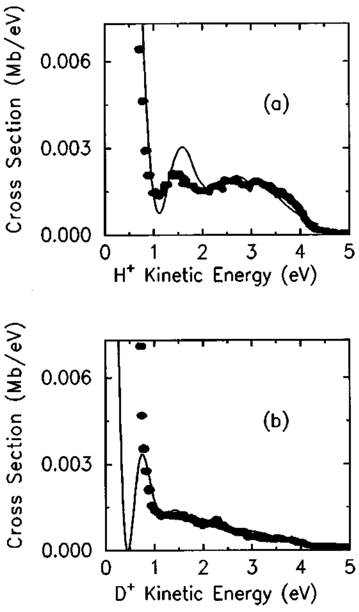

FIG. 9. Comparison between the calculated KED spectra (full line) and the experimental ones of Ref. [16] (circles) for protons and deuterons detected at 0° and $\omega=27$ eV. (a) H_2. (b) D_2.

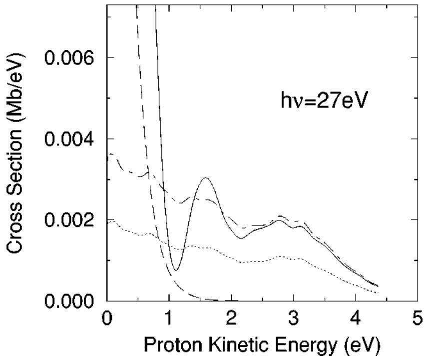

FIG. 10. Contributions to the KED spectrum of H_2 of the different terms entering the definition of the total wave function given in Eq. (31). Full line: exact results; dotted line: resonant contribution corresponding to the first term in Eq. (31); chain line: resonant contribution corresponding to the third term in Eq. (31); dashed line: nonresonant contribution corresponding to the second term in Eq. (31).

In the absence of resonant effects, the cross section decreases almost exponentially as the proton energy increases [7]. This kind of behavior is observed for the $^1\Pi_u$ continuum, which is consistent with the experimental results for $\omega\leqslant 27$ eV [16]. Resonant effects are not observed in this case because the autoionization lifetimes of the Q_1 $^1\Pi_u$ doubly excited states (see Fig. 1) are larger than the time required for dissociation. The experiment of Ref. [16] shows that in order to see resonance effects in the 90° spectrum one should go to higher photon energies ($\omega\geqslant 28$ eV), so that Q_2 $^1\Pi_u$ doubly excited states, which have a much shorter autoionization lifetime, can be excited [38]. In contrast with the $^1\Pi_u$ continuum, the KED spectrum for the $^1\Sigma_u^+$ symmetry of H_2 (see Fig. 5) shows the existence of several well-defined peaks in the whole range of photon energies investigated here (e.g., at $\omega=27$ eV there exist two peaks at $\simeq 1.5$ and 3 eV). The same peaks are obtained for D_2, but they are less apparent because the effective Franck-Condon region is smaller than for H_2 [16]. The low-energy peaks in Fig. 5 were observed very recently by Ito, Hall, and Ukai [16] and they are well reproduced in our calculations (see Fig. 9). These peaks have not been assigned in previous works. The peak at higher energies has been observed by Strathdee and Browning [10], and has been assigned to the lowest Q_1 $^1\Sigma_u^+$ resonance, which has a short autoionization lifetime [23]. The origin of the peaks observed in Figs. 5 and 7 can be explained with the help of Fig. 10 (see also Ref. [24]). This figure shows the resonant and nonresonant contributions that arise from each term in the right-hand side of Eq. (31). Three important conclusions can be extracted from this analysis. First, the nonresonant contribution exhibits the typical exponential decay of a KED spectra far from the resonance region. Second, the resonant contributions explain the existence of the high-energy peak. The same conclusion was obtained by Kirby *et al.* [12] using a local approximation and a wave function that only included the first resonant term in Eq. (31). However, note that the total resonant contribution includes the first and third terms in Eq. (31), and that the importance of both terms is comparable. The third and more important conclusion that can be extracted from Fig. 10 is that a simple incoherent addition of the resonant and nonresonant contributions does not lead to the low-energy peak. Thus the origin of such a peak lies in the strong interference between the amplitudes associated with the resonant and nonresonant parts of the wave functions. Although the existence of interference effects is not surprising (e.g., they are the basis of the Fano profiles observed in atomic photoelectron spectroscopy [39]), the large magnitude of the additional peaks in the KED spectra is quite unexpected. Indeed, they can be even more pronounced than the resonance peak itself (see, for instance, the spectrum at $\omega = 25$ eV in Fig. 5). The fact that these additional structures are not very far from the region where the cross section decreases very rapidly may explain why they have remained undetected for a long time, and why they are not seen in the experimental spectra of D_2. Indeed, in the latter case, the low-energy peaks are always below 1 eV (see Fig. 7) and the energy resolution used in the experiment is probably too small to separate them from the exponentially decreasing background. It can be also observed that, as ω increases, the positions of the peaks shift to higher energies. Moreover, at $\omega = 27$ eV and for H_2, a third peak starts to develop near the dissociation threshold, and it becomes quite apparent at 28 eV (see Fig. 5). Although its maximum lies below 1 eV, the experiment is able to reproduce the high-energy side of the peak [16]. As a conclusion, the present results show that the usual semiclassical picture in which the resonance is populated more or less efficiently, and then the nuclei separate as the superexcited molecule slides down the potential curve $E_r(R)$ toward larger internuclear separations is not substantiated. In particular, discrepancies between theoretical and experimental autoionization widths [18,19] might be due to the use of this semiclassical model to extract the widths from the measured spectra.

B. Integrated cross sections

We have integrated from 0 to $\mathcal{E}_{\max}$ the KED spectra of Figs. 5–8 for the ${}^1\Sigma_u^+$ and ${}^1\Pi_u$ symmetries and for various photon energies. $\mathcal{E}_{\max}$ is the maximum energy available for the relative nuclear motion at a given photon energy, $\mathcal{E}_{\max} = W_{g\nu} + \hbar\omega - E_0(\infty)$. The resulting total dissociative photoionization cross sections are shown in Figs. 11(a) and 12(a). As for the KED spectra, the peaks observed here come from the ${}^1\Sigma_u^+$ channel, and practically no structure is obtained in the ${}^1\Pi_u$ channel. For H_2, we have compared our results with the absolute measurements of Chung *et al.* [40]. It can be seen that both experiment and theory agree in predicting a rapid rise of the total cross section above $\omega \simeq 27$ eV. This is mainly due to resonance effects through the lowest ${}^1\Sigma_u^+$ doubly excited state. For $\omega \geqslant 30$ eV, higher doubly excited states are populated, but as they are not included in the present calculations, the theoretical cross section begins to decrease instead of keeping rising. Figures 11(b) and 12(b) also include results obtained by stopping the integration in $\mathcal{E}_f = 0.08$ eV ($\mathcal{E}_f \ll \mathcal{E}_{\max}$). For the purpose of discussion, we have also included in the figures the zero kinetic-energy spectra measured by He *et al.* [17] normalized to our results at $\omega = 20$ eV. The latter have been obtained in arbitrary units by collecting protons (and deuterons) with energy smaller than 0.01 eV ($\mathcal{E}_f = 0.02$ eV). We have not attempted to obtain a ''zero-energy'' spectrum due to the large number of points required near the dissociation threshold. However, one can see that for both H_2 and D_2 we obtain two peaks almost in the same positions as in the experiment. Furthermore, for $\mathcal{E}_f = 0.08$ eV, the shapes of both structures tend to the experimental ones. In the case of the H_2 molecule, the peak at

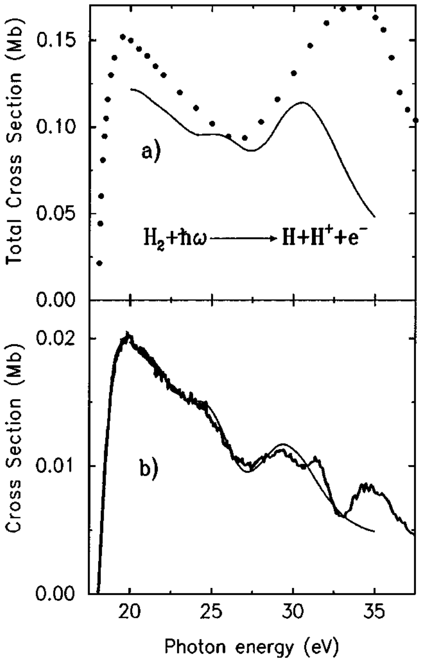

FIG. 11. Dissociative photoionization cross section of H_2 as a function of photon energy. (a) Total cross section. Line: present results; dots: experiment of Ref. [40]. (b) Thin line: present results for protons with energy smaller than 0.04 eV ($\mathcal{E}_f = 0.08$ eV); thick line: experiment of Ref. [17] for protons with energy smaller than 0.01 eV (normalized to the theory at $\omega = 20$ eV).

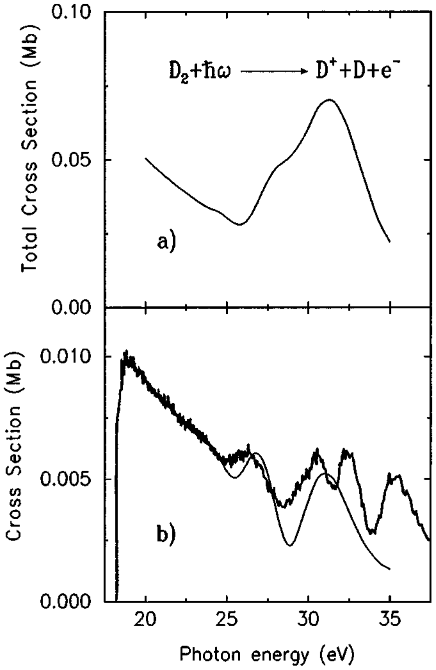

FIG. 12. Same as Fig. 11 for D_2.

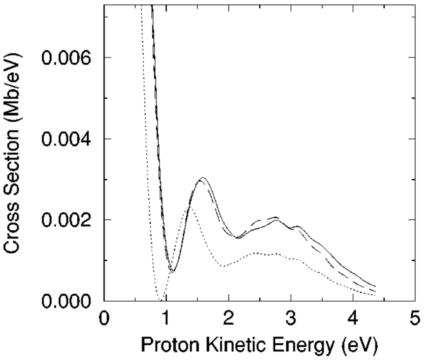

FIG. 13. Comparison between the KED spectrum of H_2 for $\omega = 27$ eV, obtained using the theory of Sec. II B (full line), the local approximation with the complete wave function of Eq. (36) (dashed line), and the local approximation with the simplified wave function of Eq. (37) (dotted line).

higher energies appear at $\omega \simeq 29$ eV, which is the energy required to populate the lowest ${}^1\Sigma_u^+$ resonance state, assuming that this state is formed in a Franck-Condon transition from the ground state [17]. The peak at lower energies is the result of the interference of the lowest ${}^1\Sigma_u^+$ resonance with the nonresonant background. In contrast with Ref. [17], we do not need to include a ${}^1\Sigma_g^+$ resonance state to account for this low-energy peak. The peaks observed at $\omega \geqslant 30$ eV correspond to resonant states not included in the present calculations. Similar conclusions can be obtained in the case of the D_2 molecule, although the resonance structures are even more pronounced.

C. Validity of the local approximation

Figure 13 shows a comparison between the KED spectrum of H_2 presented in Fig. 5 for 27-eV photons and that obtained using the local approximation (see Sec. II C). Results obtained with the theory of Sec. II B and the local approximation are very close, but those obtained with the approximate wave function (37) strongly differ from the former. Furthermore, the discrepancies between length and velocity results are much smaller for the theory presented in Sec. II B and the local approximation (around 20%) than for the local approximation that makes use of the simplified wave function (37). In the latter case, the discrepancies between gauges are of the same order of magnitude as the results themshelves. Consequently, a local approximation that makes use of Eq. (37) instead of Eq. (36) is not able to provide results to a quantitative level.

VI. CONCLUSION

We have presented a systematic study of dissociative photoionization of H_2 and D_2 for photon energies below $\simeq 30$ eV. The theoretical method makes use of B-spline functions to describe the electronic and nuclear motions, and the coupling between them. We have shown that strong interference effects between resonant and nonresonant amplitudes are responsible for the appearance of unexpected structures in the dissociative photoionization spectra of H_2 and D_2. Since these structures are the result of the quantal behavior of both electrons and nuclei, none of the semiclassical models which have been previously applied to this problem can account for the observed interference effects. Our analysis shows that the usual one-to-one correspondence between observed peaks and resonances is no longer valid to interpret dissociative photoionization spectra. Indeed, for photon energies smaller than 28 eV, the various peaks observed experimentally can be explained in terms of a single ${}^1\Sigma_u^+$ doubly excited state. We have also investigated the validity of a local approximation to evaluate the final-state wave function, and shown that it is a reasonable approximation provided that the final-state wave function includes all the resonant terms arising from the theory as well as the interference between them.

ACKNOWLEDGMENTS

This work was supported by the DGICYT Project No. PB93-0288-C02-01. I. S. acknowledges the Ministerio de Educación y Ciencia for a research contract.

APPENDIX

The asymptotic behavior of the $\xi^r_{\alpha l v E}$ wave functions defined in Eq. (23) [or alternatively in Eq. (33)] is given by [35]

$$\xi^r_{\alpha l v E} \sim \mathcal{F}(E)\exp\left[i\left(k_v R - \frac{1}{2}J\pi + \lambda_J\right)\right], \tag{A1}$$

where $\mathcal{F}(E)$ is a complex number, $k_v^2 = 2\mu[\omega - E_r(\infty)]$ (or, equivalently, $k_v^2 = 2\mu[E - W_{g\nu} - E_r(\infty)]$, with $W_{g\nu}$ the ground-state energy), and $\lambda_J = \lambda_J^R + i\lambda_J^I$ is a complex phase shift describing the scattering by a complex potential [see Eq. (23)]. From Eq. (A1), the asymptotic behaviors of the real and imaginary parts of $\xi^r_{\alpha l v E}$ are

$$\mathrm{Re}[\xi^r_{\alpha l v E}] \sim -\mathcal{A}\sin\left(k_v R - \tfrac{1}{2}J\pi\right) + \mathcal{B}\cos\left(k_v R - \tfrac{1}{2}J\pi\right), \tag{A2}$$

$$\mathrm{Im}[\xi^r_{\alpha l v E}] \sim \mathcal{B}\sin\left(k_v R - \tfrac{1}{2}J\pi\right) + \mathcal{A}\cos\left(k_v R - \tfrac{1}{2}J\pi\right), \tag{A3}$$

where

$$\mathcal{A} = \mathrm{e}^{-\lambda^I}[\mathcal{F}^R\sin\lambda^R + \mathcal{F}^I\cos\lambda^R], \tag{A4}$$

$$\mathcal{B} = \mathrm{e}^{-\lambda^I}[\mathcal{F}^R\cos\lambda^R - \mathcal{F}^I\sin\lambda^R], \tag{A5}$$

and

$$\mathcal{F} = \mathcal{F}^R + i\mathcal{F}^I. \tag{A6}$$

Equations (A2) and (A3) show that the real and imaginary components of the wave function have different amplitudes and phase shifts. By enclosing the system in a box of length $R_{\max}$, both components are forced to vanish at $R = R_{\max}$, which is not consistent with the above asymptotic behavior. This problem is solved in practice by introducing an absorbing potential in the vicinity of $R = R_{\max}$. In this work we have used an absorbing potential of the form

$$v(R)=\begin{cases}0 & \text{for} \quad R\leqslant\mathcal{R}\\ iM(R-\mathcal{R})^2 & \text{for} \quad R>\mathcal{R},\end{cases} \tag{A7}$$

where $\mathcal{R}=R_{\max}-\varepsilon_R$ (with $\varepsilon_R=1$ a.u.) and $M=30$ a.u. The large value of M ensures that all the density is absorbed before the wave function reaches the border $R=R_{\max}$. In a time-dependent picture, this avoids unphysical reflections by the potential wall at $R=R_{\max}$. Since ε_R is rather small compared to the box size, the effect of the absorbing potential is reduced to a very small region near $R=R_{\max}$. In this way, the wave function is practically unaffected for $R<\mathcal{R}$ (see Sec. III C).

[1] R. J. van Brunt and L. J. Kieffer, Phys. Rev. A **2**, 1293 (1970).

[2] A. Crowe and J. W. McConkey, Phys. Rev. B **6**, 2088 (1973); Phys. Rev. Lett. **31**, 192 (1973).

[3] J. A. Stockdale, V. E. Anderson, A. E. Carter, and L. Deleanu, J. Chem. Phys. **63**, 3886 (1975).

[4] K. Köllmann, J. Phys. B **11**, 339 (1978).

[5] J. L. Gardner and J. A. R. Samson, Phys. Rev. A **12**, 1404 (1975).

[6] A. L. Ford, K. K. Docken, and A. Dalgarno, Astrophys. J. **195**, 819 (1975).

[7] S. V. ONeil and W. P. Reinhardt, J. Chem. Phys. **69**, 2126 (1978).

[8] B. van Wingerden, Ph. E. van der Leeuw, F. J. de Heer, and M. J. van der Wiel, J. Phys. B **12**, 1559 (1979).

[9] J. L. Dehmer and D. Dill, Phys. Rev. A **18**, 164 (1978).

[10] S. Strathdee and R. Browning, J. Phys. B **12**, 1789 (1979).

[11] K. Kirby, S. Guberman, and A. Dalgarno, J. Chem. Phys. **70**, 4635 (1979).

[12] K. Kirby, T. Uzer, A. C. Allison, and A. Dalgarno, J. Chem. Phys. **75**, 2820 (1981).

[13] S. Kanfer and M. Shapiro, J. Phys. B **16**, L655 (1983).

[14] M. Landau, R. I. Hall, and F. Pichou, J. Phys. B **14**, 1509 (1981); F. Pichou, R. I. Hall, M. Landau, and C. Shermann, *ibid.* **16**, 2445 (1983).

[15] K. Ito, P. Lablanquie, P. M. Guyon, and I. Nenner, Chem. Phys. Lett. **151**, 121 (1988).

[16] K. Ito, R. I. Hall, and M. Ukai, J. Chem. Phys. **104**, 8449 (1996).

[17] Z. X. He, J. N. Cutler, S. H. Southworth, L. R. Hughey, and J. A. R. Samson, J. Chem. Phys. **103**, 3912 (1995).

[18] C. J. Latimer, K. F. Dunn, N. Kouchi, M. A. McDonald, V. Srigengan, and J. Geddes, J. Phys. B **26**, L595 (1993); J. Geddes, K. F. Dunn, N. Kouchi, M. A. McDonald, V. Srigengan, and C. J. Latimer, *ibid.* **27**, 2961 (1994).

[19] C. J. Latimer, J. Geddes, M. A. McDonald, N. Kouchi, and K. F. Dunn, J. Phys. B **29**, 6113 (1996).

[20] J. Tennyson and C. J. Noble, J. Phys. B **18**, 155 (1985).

[21] I. Shimamura, C. J. Noble, and P. G. Burke, Phys. Rev. A **41**, 3545 (1992).

[22] J. Tennyson, At. Data Nucl. Data Tables **64**, 253 (1996).

[23] I. Sánchez and F. Martín, J. Chem. Phys. **106**, 7720 (1997).

[24] I. Sánchez and F. Martín, Phys. Rev. Lett. **79**, 1654 (1997).

[25] J. N. Bardsley, J. Phys. B **1**, 349 (1968).

[26] A. U. Hazi, T. N. Rescigno, and M. Kurilla, Phys. Rev. A **23**, 1089 (1981).

[27] C. de Boor, *A Practical Guide to Splines* (Springer, New York, 1978).

[28] I. Cacelli, V. Carravetta, A. Rizzo, and R. Moccia, Phys. Rep. **205**, 283 (1991).

[29] M. Shugard and A. U. Hazi, Phys. Rev. A **12**, 1895 (1975).

[30] I. Sánchez and F. Martín, J. Phys. B **30**, 679 (1997).

[31] M. Cortés and F. Martín, J. Phys. B **27**, 5741 (1994).

[32] F. Martín, Phys. Rev. A **48**, 331 (1993).

[33] J. Damas, F. Borondo, and F. Martín, Chem. Phys. Lett. **226**, 235 (1994), and references therein.

[34] F. Borondo, A. Macías, and A. Riera, J. Chem. Phys. **74**, 6126 (1981).

[35] A. C. Allison, Comput. Phys. Commun. **3**, 173 (1972).

[36] U. V. Riss and H.-D. Meyer, J. Phys. B **26**, 4503 (1993), and references therein.

[37] I. Sánchez and F. Martín, J. Chem. Phys. (to be published).

[38] Following common notations, we have used the label Q_1 for doubly excited states converging to the $2p\sigma_u$ ionization threshold, and the label Q_2 for those states converging to the higher $2s\sigma_g$ ionization threshold.

[39] U. Fano, Phys. Rev. **124**, 1866 (1961).

[40] Y. M. Chung, E.-M. Lee, T. Masuoka, and J. A. R. Samson, J. Chem. Phys. **99**, 885 (1993).